Study of the Compressed and Expanded Liquid Rubidium with the Optimized Nonlocal Model Potential

Hong Seok Kang* and Sung Ho Park

Division of Applied Science, Jeonju University, Hyoja-dong, Wansan-ku, Chonju, Chonbuk 560-759, Korea
Received July 7, 1999

We show that Shaw's optimized nonlocal model potential (OMP) in combination with the perturbative hyper-netted-chain equation for pair correlation functions can be successfully applied to predict pair structures of compressed and expanded liquid rubidium. For compressed rubidium, it is possible to apply the OMP to a state for which the model radius is even close to the Wigner-Seitz radius. In addition, our results are parallel to those from Chihara and Kahl's quantal hypernetted-chain equation in that it supports the uniform compression model up to 6.1 GPa. Calculation also shows that the pair structure is relatively insensitive to the choice of the exchange-correlation function for the electron liquid. Discussions are also given for compressed and expanded cesium.

Introduction

Recently, we have successfully applied Shaws optimized nonlocal model potential (OMP) to the calculation of thermodynamics and pair structures of liquid alkali and alkaline-earth metals.[1] To be more precise, the calculation was based on the combination of the OMP for calculating the electronic energy of a metal[2-4] and the perturbative hypernetted-chain integral equation[5,6] (PHNC) for calculating the pair structures from a given pair potential. This success implies that the OMP, within the second-order perturbation treatment, can make a good account of the electron-ion interaction in *s-p* bonded metals. This is possible because the PHNC is sufficiently reliable to rule out any possibility that the major discrepancy from the experimental data is ascribable to the statistical mechanical part of the OMP+PHNC, *i.e.*, the PHNC. For this, we note that the PHNC is almost equally reliable for model systems interacting with a pair potential of varying degree of softness from the unscreened Coulombic system to the Lennard-Jones system.

In view of the successive description of metallic properties at normal density, a natural question is if OMP+PHNC is still reliable for liquid metals at expanded and compressed states or not. For liquid rubidium, it is possible to answer this question at least partly, since experimental data of the structure factor are available from the x-ray diffraction or the neutron scattering method. Theoretical works also suppliment the experimental observation. For compressed liquid rubidium, we mention two recent works. The first one is the first-principle molecular dynamics simulation due to Shimojo *et al.*,[7,8] and the second one is due to Chihara and Kahl (CK) on the quantal hypernetted-chain equation in combination with Rosenfeld's modified hypernetted-chain equation.[9] These works showed that the static structure factors or the radial distribution functions calculated from their methods are in good agreement with experimental data at states compressed along the melting line. In this respect, it will be interesting to answer the question to what extent the basic

idea of the model potential itself is valid when the model radius is comparable to the Wigner-Seitz radius. For this we note that the physical idea underlying the OMP is that the bare interaction of a valence electron with an ionic core can be replaced by a model potential due to Heine and Abarenkov, so that the potential yields the correct logarithmic derivative of the true wavefunction at some model radius which is small compared to the Wigner-Seitz radius. Furthermore, we need an answer to the question if the second-order perturbation theory of electron-ion interaction for *s-p* bonded metals can properly describe the dependence of the screening and the exchange-correlation effect of conduction electrons upon the change of density. On the one hand, there are many theoretical works on the pair structure of expanded liquid rubidium.[7,10-14] These works showed that a universal behavior is observed as the alkali metals are expanded along the liquid-vapor coexistence curve, many of which are related to the gradual transition from the metal to a nonmetallic state. In this respect, it will be worthwhile to study how well the present method reproduces these features.

Our previous calculations were based on Ichmaru and Utsumi's expression (IU) for the exchange-correlation function $G(k)$ of the electron liquid.[15] However, the IU expression does not give a correct asymptote at large k in that it saturates to a constant. Very recently, Moroni, Ceperley, and Senatore (MCS) presented an accurate fit to their diffusion Monte Carlo data[16] based on the correct behavior at large k. In the limit, the function takes the form $G(k) = C(k/k_F)^2 + B$, where B and C are density-dependent parameters. Although major difference in $G(k)$ is observed at $k > 2 k_F$ between the IU and the MCS, there is still a nonnegligible difference at $k < 2 k_F$, especially at $k \sim 2 k_F$. And that difference was manifested in the difference in $V(r)$ calculated from Ashcroft's empty-core pseudopotential.[17] A natural question which arises in relation to this observation is: (1) Is the difference in $G(k)$ at $k > 2 k_F$ still not important for Shaw's OMP which is nonlocal? (2) Will anything different be observed upon the change of density due to the compression or expansion? (3)

What kind of change is brought about in the pair structure as a result of change in $V(r)$? These are additional problems which will be considered in our calculation.

Formulation

In this section, we give only a brief description of the OMP and the PHNC, since the details are given in Ref. 1. The OMP is based on the optimization of the Heine-Abarenkov potential describing the bare interaction $w_0(r)$ of a valence electron with an ionic core:

$$w_0(r) = -\frac{Ze^2}{r} - \sum_{l=0}^{l_0} \Theta[R_l(E) - r]\left[A_l - \frac{Ze^2}{r}\right]P_l, \quad (1)$$

Where l_0 is the highest angular momentum quantum number for the core electrons; $R_l(E)$ and $A_l(E)$ are the radius and well-depth of the core which depend on the energy engenvalue of the system; P_l is the projection operator which extracts out the l-th angular momentum component from the eigenfunction; $\Theta(r)$ is the heavy side step function. Shaw showed that the optimization of the model wavefunction is achieved when the relation $A_l(E) = Ze^2 / R_l(E)$ is satisfied. Parameters in the model potential are calculated from the extrapolation of those for ionic term energies. Specifically, core-shift of the electron energy due to the conduction electrons and all the ions other than that to which the electron belongs was calculated from the prescriptions given by Animalu and Heine (AH),[18,19] Ballentine and Gupta (BG),[19,20] and another one based on the BG, which will be explained in the next section.

In the context of the second-order perturbation theory, the effective interaction $V(r)$ between a pair of ions is the sum of direct and indirect contributions. Namely,

$$V(r) = \frac{(Z^*e)^2}{r} + \frac{\Omega}{\pi^2}\int_0^\infty dq q^2 F(q)\frac{\sin(qr)}{qr}, \quad (2)$$

Where Z^* is the effective valence which takes into account the difference between the true wavefunction and the model pseudo wavefunction, and $F(q)$ is the energy-wavenumber characteristic. To calculate $F(q)$, we assume a uniform distribution of the depletion charge over an appropriate core volume. As explained in the previous section, the exchange-correlation function $G(k)$ comes into our calculation through two different expressions due to MCS and IU.

In the PHNC, the pair potential $V(r)$ is divided into the reference potential $V_0(r)$ and the perturbation contribution $V_1(r)$ in a way that depends on the density. As in the previous work, the repulsive range λ in $V_0(r)$ is assumed to follow the relation $\lambda = min(a_{fcc}, r^*)$, where a_{fcc} is the nearest neighbor distance in the face-centered-cubic lattice and r^* is the interionic distance at which $V(r)$ becomes the global minimum. Next, the bridge function $B(r)$ of the metallic system is approximated by that, $B_0(r)$, for the reference system. In turn, $B_0(r)$ is calculated from the numerical solution of the Ornstein-Zernike relation using Ballone *et al*'s closure relation.[21]

Results and Discussion

First, we describe our calculations for liquid rubidium compressed along the melting line. Five states considered in Table 1 correspond to those for which experimental data of pair structure are available.[22] An important observation from the Table is that the relation $R_1 < a_{WS}$ is not satisfied at (570 K, 6.1 GPa) with neither the AH nor the BG set of the OMP parameters. This can be a serious drawback of the OMP, since the method is expected to work only if the potential due to an ionic core becomes Coulombic within the Wigner-Seitz radius. The condition can be expressed as $R_c < R_l < a_{WS.}$ (R_c is the core radius of Rb$^+$ ion.) However, it is also possible that it merely reflects the fact that both of the AH and the BG fail to give reasonable estimation of the core-shift $\Delta\varepsilon_F$ for the metallic environment at high compression. Therefore, we propose a modified BG scheme (M-BG) in which $\Delta\varepsilon_F$ for all values of l are calculated from the BG expression for $l = 0$. For this, we mention an important aspect of Shaw's formalism: Values of A_l from the AH or the BG are not used as they are, but are modified to take into account additional terms to the first order in the total model potential. [For more details, see Eqs. (5)-(10) in Ref. 3.] Not to say, the major reason for doing this is that we need more accurate estimation of the core-shift than simply taking the average of the potential for an electron in the Wigner-Seitz cell. Therefore, it remains a question if various arguments used to derive the BG expression for $\Delta\varepsilon_F$ are still valid in our calculation as they are. Furthermore, there are various approximations in the BG. For example, it does not take into account the inhomogeneity of the electron system originating from the large electronic density inside an ionic core. In short, we believe that our modification to the BG does not introduce any serious problem in the calculation. In fact, difference in R_1 between the M-BG and the BG is less than two percent, which is much smaller than that between the AH and the BG. As shown in Table 1, at (570 K, 6.1 GPa), R_1 (E_F) calculated from this modified scheme satisfies the relation $R_c < R_1 < a_{WS}$.[23]

For clarity, we have studied the dependence of $V(r)$ and pair structures on different choice of $G(k)$ as well as on dif-

Table 1. Model radii $R_l(E_F)$ in the OMP at $l = 0$ and 1 for liquid rubidium compressed along the melting line. Three different sets of data corresponds to different methods for calculating the core-shift. BG, M-BG, and AH denote the methods due to Ballentine and Gupta, our modification of that due to BG, and Animalu and Heine. The Wigner-Seitz radius a_{WS} at each density is shown for comparison. Note that the optimization of the model wavefunction requires that $A_l(E_F) \cdot R_l(E_F) = Ze^2$, where Z is the valence charge.

T(°K)	ρ (g/cc)	P(GPa)	$R_0(E_F)$			$R_1(E_F)$			a_{WS}
			BG	M-BG	AH	BG	MBG	AH	
350	1.459	0.0	4.141	4.141	4.372	4.297	4.263	4.391	5.391
370	1.562	0.2	4.144	4.144	4.396	4.302	4.265	4.403	5.271
520	2.057	2.5	4.121	4.121	4.472	4.301	4.253	4.439	4.810
540	2.276	3.9	4.171	4.171	4.605	4.337	4.281	4.498	4.649
570	2.850	6.1	4.198	4.198	4.847	4.368	4.296	4.588	4.313

ferent choice of the parameters in the OMP. Different combinations will be denoted by (M-BG, MCS), (M-BG, IU), (BG, MCS), (BG, IU), (AH, MCS), and (AH, IU). As explained in the previous sections, M-BG, BG, and AH denote the different methods for extracting the core-shift, and MCS and IU represent the difference in the calculation of the exchange-correlation function $G(k)$. When we consider the effect of $G(k)$ on $V(r)$, we observe a behavior which is qualitatively very similar to that observed by Moroni *et al.* for liquid sodium calculated from the local pseudopotential.[17] At (350 K, 0 GPa), corresponding to the triple point, Figure 1 shows that the MCS $V(r)$ is lower than the IU by almost a constant amount ($\sim$0.18 kT) at $r^* < r < r_s$, where $V(r_s)$ corresponds to the shoulder in the potential. This difference (in units of kT) gets smaller as pressure increases. [See Figure 2 for $V(r)$ at (540 K, 3.9 GPa).] From the two figures, we also observe that the difference in $V(r)$ introduced by the modification of the BG to the M-BG is much smaller than that due to change of $G(k)$ or due to the change of the OMP parameters from the AH to the BG, being noticeable only at $r \sim r^*$. Fortunately, this implies that possible error in $V(r)$ introduced by a few percent of inaccuracy in the OMP parameters is not significant. Rather, much larger uncertainty can be introduced
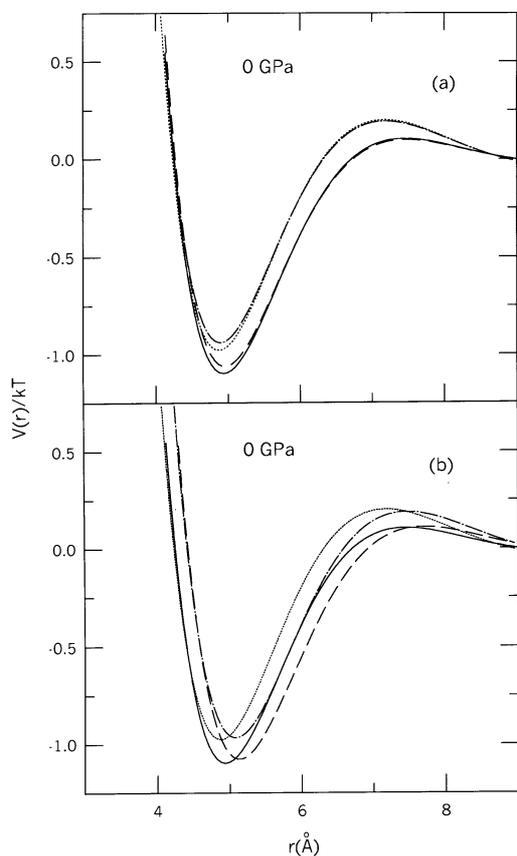
through the small uncertainty in our knowledge of $G(k)$. For $k < 2\,k_F$, we note that the only appreciable difference in $G(k)$ is observed at $k \sim 2\,k_F$ among various expressions for it available up to now. [See Figure 4 of Ref. 17.] As in the case of the local pseudopotential, the uncertainty at larger k is not important. This is supported by our calculation which shows that the curves of $V(r)$ from the MCS and the local density approximation (LDA) are nearly indistinguishable from each other on the scale shown in Figure 1.

Figure 3 shows the structure factor calculated from the present method in comparison with Tsuji *et al*'s experimental data[22] at four compressed states considered in Table 1. For simplicity, our results are shown for (M-BG, MCS) and (AH, MCS) only. It is practically impossible to distinguish (M-BG, IU), (BG, MCS), (BG, IU) from the (M-BG, MCS) on the scale shown in the figure. Presumably, this result reflects the well-known fact that the structure of liquid is mainly determined by its repulsive interaction, noting that the major difference in $V(r)$ between these four combinations occurs only in the attractive range. On the other hand, difference in $V(r)$ between the AH and the BG extends to the repulsive range, causing much larger difference in the pair structure. In the figure solid lines correspond to the M-BG, and the dotted lines, to the AH. In accordance with our previous work on the liquid alkali metals at normal pressure, the AH exhibits larger oscillation in the first few extrema. We
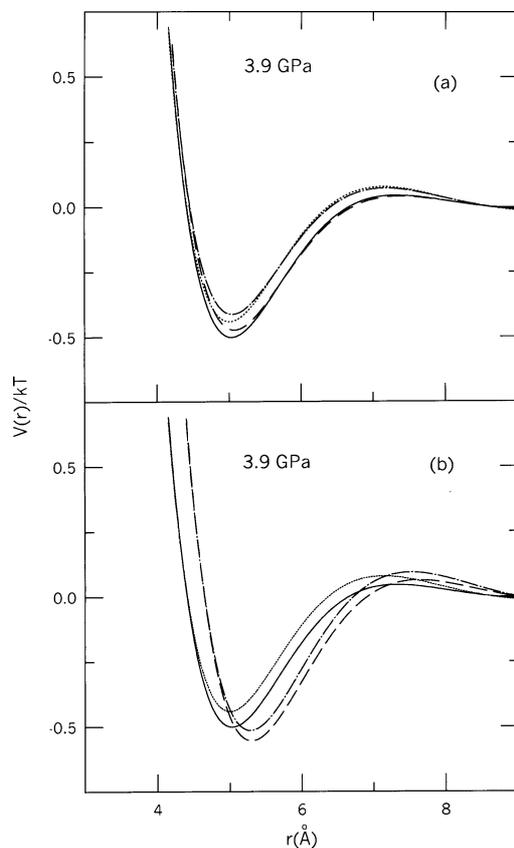
Figure 1. Pair potential $V(r)$ for liquid rubidium at (350 K, 1.459 g/cc, 0 GPa) calculated from the OMP: (a) Solid, dotted, dashed, and dash-dot-dashed lines correspond to (M-BG, MCS), (M-BG, IU), (BG, MCS), and (BG, IU), respectively. (b) Solid, dotted, dashed, and dash-dot-dashed lines correspond to (M-BG, MCS), (M-BG, IU), (AH, MCS), and (AH, IU), respectively. See the text for definitions of these terms.

Figure 2. Pair potential $V(r)$ for liquid rubidium at (540 K, 2.276 g/cc, 3.9 GPa) calculated from the OMP. See the caption in Figure 1 for the notation.
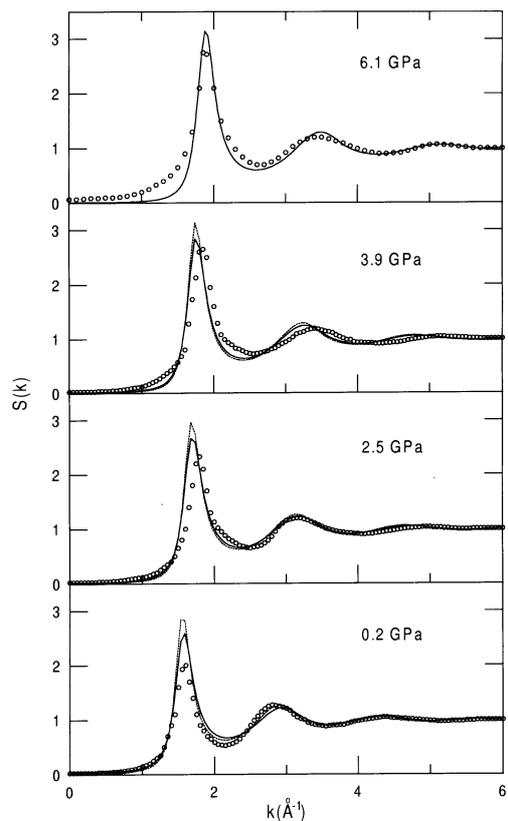
Figure 3. $S(k)$ for the liquid rubidium at four states (0.2, 2.5, 3.9, and 6.1 GPa) compressed along the melting line calculated from the present method in comparison with Tsuji *et al*'s experimental data[22] (open circles). Solid and dotted lines correspond to the M-BG and the AH sets of the OMP parameters. At 6.1 GPa the AH data are not shown, since $R_1 > a_{WS}$. See the text.

have not shown the AH result at 6.1 GPa, since R_1 becomes larger than a_{WS} as described above.

More importantly, our results are qualitatively very similar to those of Chihara and Kahl (CK) calculated from the quantal hypernetted-chain equation in conjuction with the MHNC for calculating the pair structure.[9] Keeping in mind that the low k behabior of the experimental data are rather uncertain,[9] we find a good agreement with experimental data at 0.2 and 6.1 GPa. However, theoretical peak positions are shifted toward smaller k at 2.5 and 3.9 GPa. CK also observed a similar behavior, and they attributed it to the possible inaccuracy of the estimated density of liquid rubidium at high pressure. In fact, the peak position calculated from the M-BG or the BG agrees with experimental data much better if the density is slightly increased. Figure 4 shows this at 3.9 GPa. Theoretical data in the figure were calculated at $\rho =$ 2.560 g/cc corresponding to the decrease in a_{WS} by approximately 4%. We still note that there remains a noticeable difference in the height of the first two maxima. According to Tsuji, there is some ambiguity in the experimental values of the peak height, while the peak position is accurate and reliable.[9] Figure 5 shows $g(r)$ calculated from the present method in comparison with that from the Fourier trasnsform of Tsuji *et al*'s experimental $S(k)$ at 0, 2.5, and 6.1 GPa. In Refs. 7
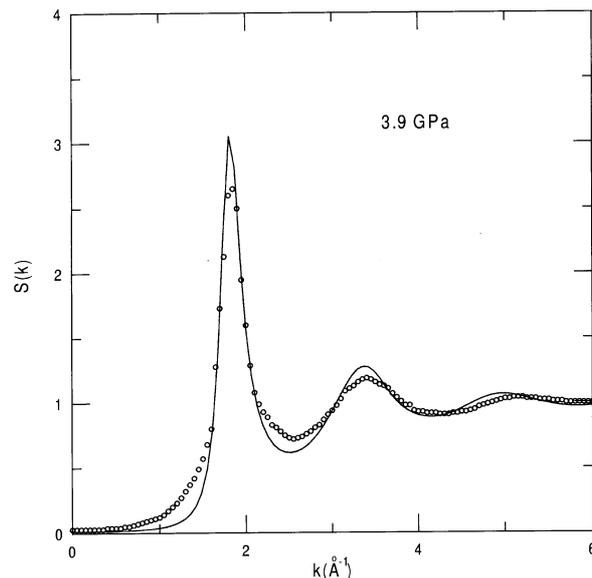

Figure 4. $S(k)$ for the liquid rubidium at 3.9 GPa calculated from the present method in comparison with Tsuji *et al*'s experimental data[22] (open circles). Solid line represents our data from the M-BG at 2.560 g/cc.
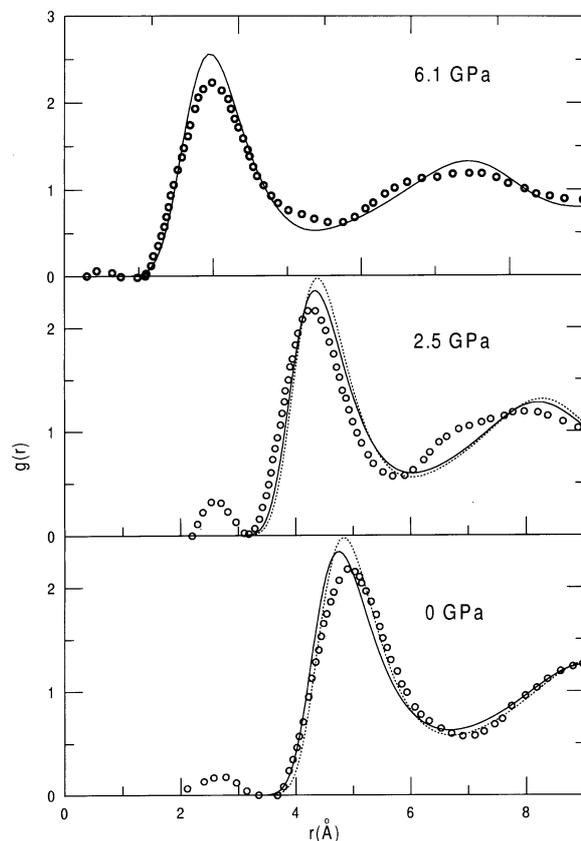

Figure 5. $g(r)$ for the liquid rubidium at 0, 2.5, and 6.1 GPa calculated from the present method in comparison with Tsuji *et al*'s experimental data[22] (open circles). Solid and dotted lines represent our data from the M-BG and the AH sets of the OMP parameters.

and 8, similar comparison was given for Shimojo *et al*'s result obtained from the first-principle simulation. It should be mentioned again that $g(r)$ derived from the experimental

$S(k)$ is subject to some uncertainty. Keeping this in mind, we conclude that our data agree with experimental data in a reasonable way and exhibit a behavior again very similar to Shimojo *et al*'s results. Unfortunately, the uncertainty of the experimental data makes it difficult to evaluate the reliability of the AH relative to the BG or the M-BG. At present, any of them seems to be about equally reliable as long as the density does not exceed 1.5 times of that at the triple point.

It is also worth mentioning that the OMP still gives reliable results at high pressure, even in case when the model radius is very close to the Wigner-Seitz radius. For example, at 3.9 GPa, Table 1 shows that both of R_0 (E_F) and R_1 (E_F) already exceed 90% of the Wigner-Seitz radius in all three methods of choosing the OMP parameters. Second, the present calculation was performed without modeling or pseudizing the *d*-component of the valence wavefunction. According to Shimojo *et al*'s calculation, the electronic $s - d$ transition takes place gradually as the pressure increases. As a result, the electronic density of state near the Fermi level consists mainly of *s* component at 0 GPa, and *d* component at 6.1 GPa. At present, the uncertainty of the experimental data does not allow us to figure out what is lost by not modelling the *d*-component of the wavefunction. It's possible that the lowest *d*-orbital is already smooth enough not to need modellization .

CK pointed out that there is a strong scaling property in the structure of compressed liquid alkali metals in that $S(k)$ of two different states practically coincides when the distance is scaled in units of a_{WS}. Figure 6 shows that our calcu-
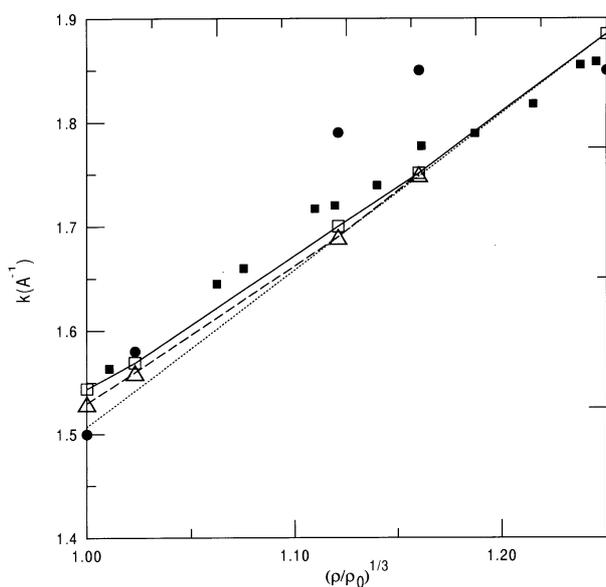
lation also supports this observation. As noted by them, the first peak of $S(k)$ is located almost at the same scaled position ($k_1 a_{WS} = 4.30$) at all the states considered. Specifically, we see no sign of deviation from the uniform compression model at 6.1 GPa. This is in contrast to Shimojo *et al*'s conclusion that the liquid rubidium deviates from the uniform compression model at 6.1 GPa, which was ascribed to the electronic $s - d$ transition described above. Although not shown here, the uniform compression model is further supported by our finding that the peak position in $g(r)$ is inversely proportional to $\rho^{1/3}$. More detailed investigation shows that this scaling property is not attributable to the scaling property of the pair potential: We are able to confirm that plots of $V(r)/kT$ versus r/a_{WS} at various pressures do not coincide with each other. Rather, Figure 7 supports CK's observation that $V(r)$ is almost state-independent, although ours are slightly more sensitive to the change of density. [See Figure 8 of Ref. 9 for comparison.]

Now, we briefly consider liquid rubidium expanded along the liquid-vapor coexistence curve up to (1900 K, 0.64 g/cc). As an example, Figure 8 shows $V(r)$ for (M-BG, MCS), (M-BG, IU), (AH, MCS), and (AH, IU) at (1400 K, 0.97 g/cc). Curves for the BG are not shown, since they are nearly indistinguishable from those for the M-BG. Although less pronouncd, the variation of $V(r)$ with variations of $G(k)$ and the OMP parameters is qualitatively similar to that at 350 K shown in Figure 1. Figures 9 and 10 show $S(k)$ and $g(r)$ calculated from the present method in comparison with Franz *et al*'s experimental data[24] at 1400 K. We first note that four theoretical curves of $S(k)$ are in reasonable agreement with experimental data, differing from each other only at $k \sim 0$. Similar degree of reliability is also manifested in the theoretical $g(r)$. Interestingly, all the curves exhibit a behavior qualitatively very similar to Shimojo *et al*'s result from the first-
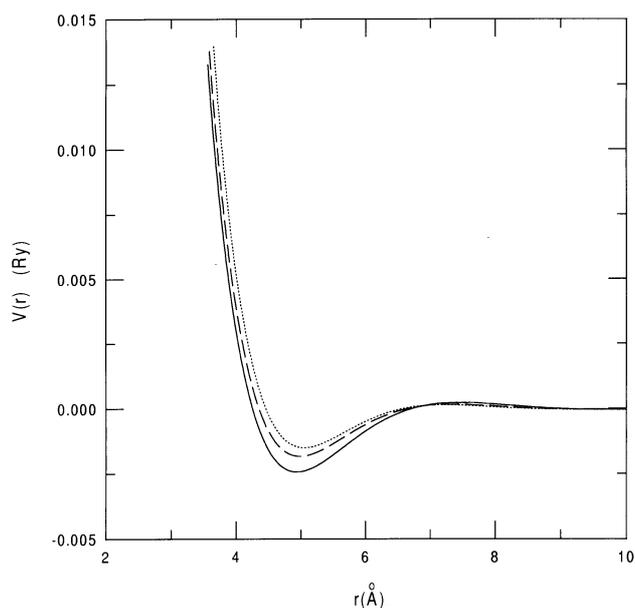

Figure 6. Peak position, k_1, of $S(k)$ at states compressed along the melting line. Filled circles are Tsuji *et al*'s experimental data at 0, 0.2, 2.5, 3.9, and 6.1 GPa. Filled squares are also from Tsuji *et al*'s experiments. These data are digitized from Figure 11 of Ref. 9. Dotted line represents Chihara and Kahl's empirical rule $k_1 a_{WS} = 4.30$ deduced from their QHNC calculation.[9] Open squares connected by a solid line correspond to the present calculation based on the M-BG set of the OMP parameters. Open triangles connected by a dashed line are for the AH. Theoretical datum is not shown for the AH at 6.1 GPa, since $R_1 > a_{WS}$.

Figure 7. Pair potential $V(r)$ for liquid rubidium at 0 (solid line), 2.5 (dashed line), and 6.1 GPa (dotted line) calculated from the OMP based on the (M-BG, MCS).
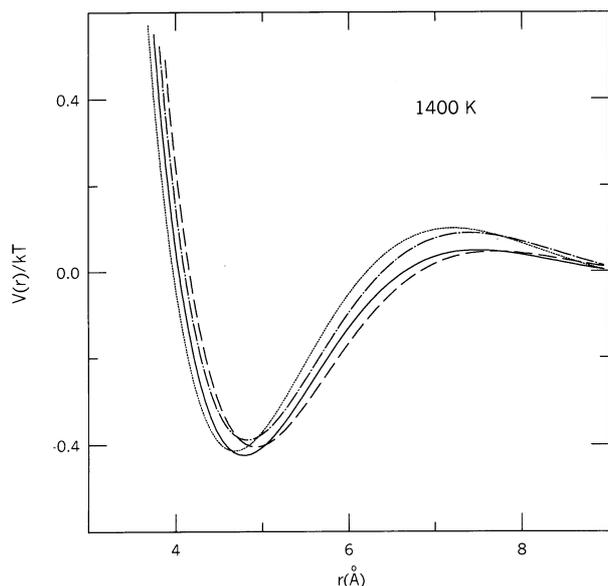
Figure 8. Pair potential $V(r)$ for liquid rubidium at (1400 K, 0.97 g/cc) calculated from the OMP. See the caption in Figure 1(b) for the notation.
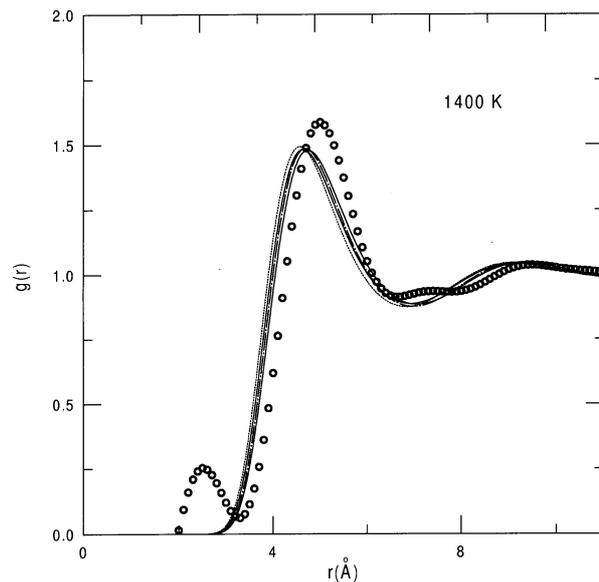

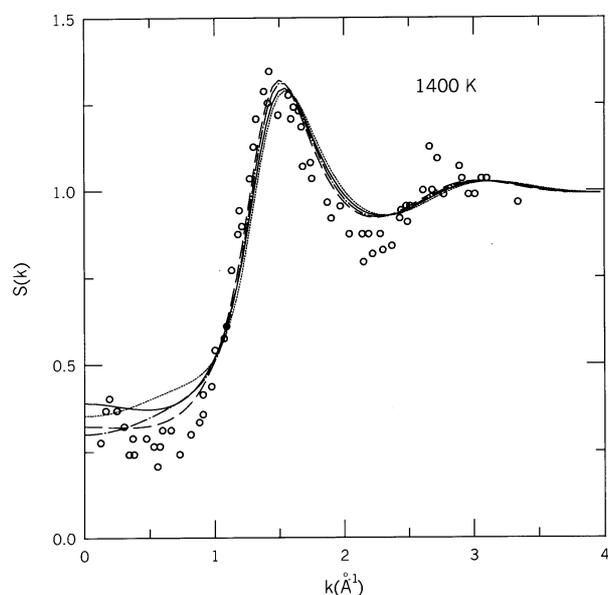**Figure 10**. $g(r)$ for rubidium at (1400 K, 0.97 g/cc). Notations are the same as in Figure 1(b).

Figure 9. $S(k)$ for liquid rubidium at (1400 K, 0.97 g/cc) calculated from the OMP. See the caption in Figure 1(b) for the notation.

Figure 11. The first coordination number N_1 of the liquid rubidium expanded along the liquid-vapor coexistence curve. Open circles, filled circles, open triangles, and filled triangles denote results from the present calculation based on the (M-BG, MCS), (AH, MCS), (M-BG, IU), and (AH, IU), respectively. Solid and dotted lines show the best fits to the (AH, MCS) and (M-BG, IU).

principle simulation shown in Figure 1 of Ref. 14. We list two more results consistent with experimental results which are universal to all the alkali metals. First, the peak position, k_1, in $S(k)$ is almost invariant under change in density. Similarly, the peak position, r_1, in $g(r)$, decreases only slightly with decrease in density. Second, the first coordination number N_1 decreases linearly with decrease in density, as shown in Figure 11. [Here, N_1 is defined by $2\rho \int_0^{r_1} dr 4\pi r r^2 g(r)$.] In short, all the six combinations of various expressions for $G(k)$ and the OMP parameters can be considered to give pair structures almost equally reliable for the expanded rubidium, taking the large uncertainty in the experimental data of $S(k)$ into account.
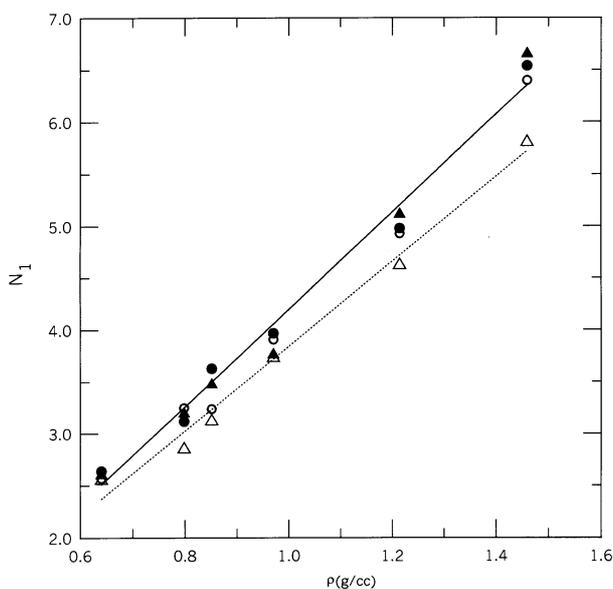
It is also possible to apply the present method to other liquid metals. For this, we note that Tsuji *et al.* performed X-ray diffraction study of the dependence of the structure factor of liquid cesium on the pressure.[25] They argued that there is a structural change at about 2 GPa, and another one between 3 and 4 GPa. The latter change was related to the decrease in the peak height of the structure factor at 4.3 GPa compared to that at the lower pressure. The change at 2 GPa was ascribed to a transition from bcc-like structure to fcc-like one. Related to this problem, we have made preliminaty calculations at four compressed states considered in the

experiment. For this, we first made an estimation of the density of these states using Harrison's local pseudopotential, in combination with the Gibbs-Bogoliubov inequality based on the soft-sphere reference system.[26] Reliability of the method was partly confirmed by its good ability to reproduce the experimental PVT relation up to 1.8661 GPa within 1% of Marenkov *et al*'s data.[27] However, it should be also mentioned that there exists a large uncertainty in the value of experimental volume at high pressure. In fact, the volume estimated by Kuchhal *et al.* is different from that due to Marenkov *et al.* by about 15% at (473.15 K, 1.8661 GPa), which corresponds to the state of the highest pressure considered in Table 3 of Ref. 27. In short, our calculations for the OMP+PHNC were carried out at (373.15 K, 2.022 g/cc, 0.2 GPa), (484.15 K, 2.856 g/cc, 1.6 GPa), (483.15 K, 3.357 g/ccc, 2.9 GPa), and (485.15 K, 3.784g/cc, 4.3 GPa). For three states up to 2.9 GPa, our calculation supports the following experimental observations: (1) The height of the first peak in $S(k)$ increases with pressure. (2) The peak position of $S(k)$ increases with pressure, while the peak position, r_1, of $g(r)$ decreases. Furthermore, our values of r_1 (= 5.007, 4.468, and 4.328 at these states) agree with experimental data shown in Figure 4 of Ref. 25. (3) Values of the first coordination number (= 6.59, 7.65 and 7.36) exhibit a maximum at 1.6 GPa. Unfortunately, the M-BG model radius, $R_0(E_F)$ and $R_1(E_F)$, becomes greater than the Wigner-Seitz radius at 4.3 GPa. At present, it is not clear if this is due to the error in the estimated density or due to the limitation of the OMP itself. In short, pair structures calculated from the present method are also in reasonable agreement with experimental data for compressed liquid cesium. Similarly to the case of expanded rubidium, calculation on the expanded cesium also shows universal features of the alkali metals related to the metal-nonmetal transition, which we do not show here explicitly.

Conclusion

We have shown that an *ab initio* method based on the combination of the OMP and the PHNC can successfully describe pair structures of liquid rubidium compressed along the melting line. These are even the cases at 3.9 and 6.1 Gpa, where the model radii in the OMP exceed 90% of the Wigner-Seitz radius. In these states, our calculations are made possible through the modification of the method for calculating the OMP parameters due to Ballentine and Gupta. An important observation is that our calculation supports Chihara and Kahls finding that the liquid rubidium is compressed uniformly as it is compressed along the melting line. Preliminary calculation also shows that the present method can be used for the study of liquid cesium under compression.

When applied to the systems of liquid rubidium and cesium expanded along the liquid-vapor coexistence curve, our calculation reproduces universal features common to all alkali metals which are observed as the metal-nonmetal tran-

sition is gradually approached. We have also observed that the pair potentials and the pair structures are slightly dependent on the different choice of the exchange-correlation function, as well as on different choice of the core-shift used to evaluate the OMP parameters.

References

1. Kang, H. S. *Phys. Rev. B* **1999**, *60*, 6362.
2. Shaw, R. W. *Phys. Rev.* **1968**, *174*, 769.
3. Shaw, R. W. *J. Phys. C* **1969**, *2*, 2335.
4. Shaw, R. W. *J. Phys. C* **1970**, *3*, 1140.
5. (a) Kang, H. S.; Ree, F. H. *J. Chem. Phys.* **1995**, *103*, 3629. (b) Kang, H. S.; Ree, F. H. *J. Chem. Phys.* **1995**, *103*, 9377.
6. Kang, H. S.; Ree, F. H. *Phys. Rev. E* **1998**, *57*, 5988.
7. Hoshino, K.; Shimojo, F. *J. Phys.: Condens. Matter* **1996**, *8*, 9315.
8. Shimojo, F.; Zempo, Y.; Hoshino, K.; Watabe, M. *Phys. Rev. B* **1997**, *55*, 5708.
9. Chihara, J.; Kahl, G. *Phys. Rev. B* **1998**, *58*, 5314.
10. Gonzalez, D. J.; Ng, D. A.; Silbert, M. *J. Non-Cryst. Solids* **1990**, *117-118*, 469.
11. Matsude, N.; Mori, H.; Hoshino, K.; Watabe, M. *J. Phys.: Condens. Matter* **1991**, *3*, 827.
12. Jakse, N.; Bretonnet, J. L. *J. Non-Cryst. Solids* **1993**, *156-158*, 149.
13. Chen, H. C.; Lai, S. K. *Phys. Rev. E* **1994**, *49*, R982.
14. Shimojo, F.; Zempo, Y. *Phys. Rev. B* **1995**, *52*, 9320.
15. Ichimaru, S.; Utsumi, K. *Phys. Rev. B* **1981**, *24*, 7385.
16. Moroni, S.; Ceperley, D. M.; Senatore, G. *Phys. Rev. Lett.* **1995**, *75*, 689.
17. Senator, G.; Moroni, S.; Ceperley, D. M. *J. Non-Cryst. Solids* **1996**, *205-207*, 851.
18. Animalu, A. O. E.; Henie, V. *Philos. Mag.* **1965**, *12*, 1249.
19. Cowley, E. R. *Can. J. Phys.* **1976**, *54*, 2348.
20. Ballentine, L. E.; Gupta, O. P. *Can. J. Phys*. **1971**, *49*, 1549.
21. Ballone, P.; Pastore, G.; Galli, G.; Gazzillo, D. *Mol. Phys*. **1986**, *59*, 275.
22. Tsuji, K.; Katayama, Y.; Morimoto, Y.; Shimomura, O. *J. Non-Cryst. Solids* **1996**, *205-207*, 295.
23. The core radius (= 2.82 Å) was taken from Table 4 of Ref. 18, which was deduced from the lattice spacing of ionic crystals.
24. Franz, G.; Freyland, W.; Glazer, W.; Hensel, F.; Schneider, E. *J. Phys*. (Paris) **1980**, *41*, C8-194.
25. Tsuji, K.; Yaoita, K.; Imai, M.; Mitamura, T.; Kikegawa, T. *J. Non-Cryst. Solids* **1990**, *117-118*, 72.
26. Moriarty, J. A.; Young, D. A.; Ross, M. *Phys. Rev. B* **1984**, *30*, 578.
27. Kuchhal, P.; Kumar, R.; Daas, N. *Phys. Rev. B* **1997**, *55*, 8042.